Grazing-incidence antireflection films. I. Basic theory

J. P. Hannon, N. V. Hung, and G. T. Trammell
Physics Department, Rice University, Houston, Texas 77251

E. Gerdau, M. Mueller, R. Rüffer, and H. Winkler
Institut für Experimentalphysik, Universität Hamburg, Hamburg, Germany

(Received 9 May 1984)

We discuss the possibility of a new interference technique for x-ray and γ-ray optics—the simple idea of grazing-incidence antireflection films (GIAR films)—for creating high-efficiency antireflection coatings for near-grazing-incidence reflection of hard x rays and γ rays. The motivation is the possible application to producing "ultranarrow" bandpass filters for synchrotron radiation with frequency widths $\approx 10^{-8}$—10^{-6} eV, giving a unique high-resolution, long-coherence-length, x-ray source for probing soft inelastic excitations and opening up new possibilities in x-ray interferometry. In this first of two papers on nonresonant GIAR films, we develop the basic theory and discuss in detail the simplest ideas for achieving antireflection films—impedance-matched quarter-wave films and damping stabilized solutions—which can both be obtained by coating a high-density mirror with a single lower-density film.

I. INTRODUCTION

Thin-film interference techniques are of central importance in modern optics. In the optical region, thin dielectric films are used to produce antireflection coatings, broad and narrow bandpass frequency filters, polarizers, dichroic mirrors for color-selective beam splitting, and multilayer high-reflectance dielectric mirrors. The technology and application of such thin-film devices have expanded dramatically during the last 30 years.[1–6]

In x-ray optics, smooth multilayer films are now being developed to produce x-ray mirrors for soft x rays in the (100—200)-Å region, with potential application to the construction of normal-incidence x-ray reflecting telescopes and microscopes, as well as broad bandpass filters, polarizers, and beam deflectors.[7–11]

In neutron optics, multilayer "supermirrors" have been proposed to extend by several times the grazing-incidence critical angle θ_c for use in neutron polarizers and for focused mirror systems.[12,13]

The purpose of this paper is to discuss the possibility of a new interference technique for x-ray and γ-ray optics—the simple idea of grazing-incidence antireflection films (GIAR films)—for creating high-efficiency antireflection coatings for near-grazing-incidence reflection of hard x rays and γ rays.[14]

The primary motivation for this study is the possible application to γ-ray optics: using GIAR films to eliminate the nonresonant electronic reflection from a resonant mirror offers a new technique for obtaining pure nuclear, coherent γ-ray scattering.[14] If such pure resonant scattering can be achieved, an immediate application would be an "ultranarrow" bandpass filter for synchrotron radiation. The resulting beam would be highly monochromatic ($\Delta\omega \approx 10^{-8}$—$10^{-6}$ eV) with a potential brightness greatly exceeding that available from natural γ-ray sources. Such a source would offer a unique high-resolution x-ray probe of "soft" inelastic excitations ($\Delta\omega \lesssim 10^{-6}$ eV), opening up a new region inaccessible by other scattering methods. There would also be immediate applications to Mössbauer experiments involving coherent scattering from perfect crystals, structure determination of biomolecules, and studies of surface magnetism. Also, the long coherence length of the signal (≈ 30 m) could offer quite new possibilities in x-ray interferometry.

The basic idea of GIAR films is as follows: In x-ray optics, the small index-of-refraction decrease ($N_0=1 \rightarrow N_1=1-2\pi\lambda^2 n Z r_0 \cong 1-10^{-5}$, where n is the atomic density, Z is the atomic number, and $r_0=e^2/mc^2$), on entering a medium of higher electron density, produces near-total reflection of x rays at grazing incidence on a flat surface.[15] The critical angle is $\varphi_c=(n\lambda^2 Z r_0/\pi)^{1/2}$. For $\varphi > \varphi_c$, there is a rapid dropoff in reflected intensity with increasing φ and a rapid increase in the penetration depth $l_\perp(\varphi)$. For ^{56}Fe and 14.4-keV radiation, $\varphi_c = 3.8$ mrad, and for $\varphi = 3.0$ mrad, $|R|^2 \simeq 0.9$ and $l_\perp \simeq 29$ Å, while at $\varphi = 4.5$ mrad, $|R|^2 \simeq 0.1$ and $l_\perp \simeq 472$ Å.

For $\varphi > \varphi_c$, where deep penetration occurs, it should be possible to strongly suppress the x-ray reflection with an impedance-matched quarter-wave film, just as in the optical coating of lenses. That is, the mirror is coated with a film of proper impedance such that the reflections at the upper and lower interfaces are equal, with the thickness chosen so that the two waves emerge 180° out of phase. The quarter-wave-film condition gives $l_\perp(\varphi)=\frac{1}{4}\lambda(\varphi^2-\varphi_c^2)^{-1/2}$, which is typically ≈ 50—100 Å. A quarter-wave film for 1-Å radiation is possible because grazing incidence augments the required film thickness by the factor $(\varphi^2-\varphi_c^2)^{-1/2}$. In addition to impedance-matched quarter-wave GIAR films, we will see that new "damping-stabilized" solutions arise due to the effect of strong photoabsorption.

The fact that x-ray interference between interface re-

flections can occur at grazing incidence was observed in 1930 by Kiessig[16] who found half-wave-film interference fringes for grazing-incidence reflection from a film of Ni on glass. Important extensions in theory and experiment have been made by Alichanow and Arzimowic,[17] Parratt,[18] Rieser,[19] and Segmüller.[20] As pointed out in these papers, the fringe pattern gives a sensitive measure of film thickness and index of refraction, and offers a probe of surface properties involving variations of electron density with depth. Of course, in these investigations there was no interest in eliminating reflections, so the possibility of antireflection coatings has not been studied.

In this paper we first give a brief review in Sec. II of the theory of grazing-incidence reflection from layered media. In Sec. III we consider the simplest case of a high-density mirror coated with a single lower-density film. We show there are two possible antireflection solutions—impedance-matched $\lambda/4$ films, and an alternate set of damping stabilized solutions which arise due to photoabsorption. We also examine the effects of long-range film-thickness variations, incident-beam divergence, and the frequency range of suppression.

In the following paper II,[21] we discuss alternative techniques for suppressing electronic reflections with half-wave films, ultrathin films, tapered impedance films, and general multilayer techniques. In forthcoming papers we examine the following topics. The theory of pure nuclear, coherent γ-ray reflections using GIAR films is discussed in paper III,[22] and the application to resonant filtering of synchrotron radiation is discussed in paper IV.[23] In paper V,[24] we discuss the related idea of resonant superlattice GIAR mirrors which have multiple resonant layers to enhance resonant scattering at larger incidence angles several times ϕ_c. Finally, in paper VI,[25] we discuss two questions of particular importance for producing high-efficiency antireflection films—the effect of surface and volume "roughness" and the limitations imposed by "noise" arising from various sources of incoherent scattering.

II. REFLECTION FROM LAYERED MEDIA

Grazing-incidence reflection of x rays from layered media was first given a general treatment by Parratt.[18] Also, except for the effects of strong x-ray photoabsorption, the mathematical problem is the same as for reflection of optical radiation from layered dielectric films.[1–6]

A. Grazing incidence reflection

As was first pointed out by Compton,[15] critical reflection of x rays is possible due to the small index-of-refraction decrease in going to a medium of higher electron density. The same results, from a different viewpoint, can be derived directly from the dynamical theory of x-ray and γ-ray optics.[26–28] Here we take the index-of-refraction approach. The dynamical development, which is particularly convenient for treating the effects of surface irregularity, is discussed in Appendix A.

For x-ray radiation incident near grazing incidence on a flat surface as shown in Fig. 1(a), translational invariance implies that the (x,y) components of the reflected and transmitted wave vectors must remain unchanged. The incident wave is $\hat{\epsilon}_0 \exp(ig_0 z)$, where

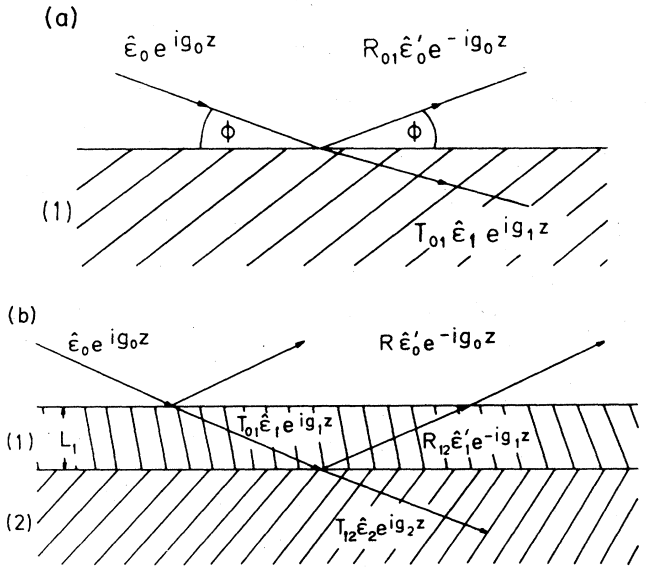

FIG. 1. Grazing-incidence geometry.

$$g_0 = k_0 \phi \tag{1}$$

is the z component of the incident wave vector; the reflected wave is $R_{01}\hat{\epsilon}'_0 \exp(-ig_0 z)$ and the transmitted wave in medium 1 is $T_{01}\hat{\epsilon}_1 \exp(ig_1 z)$. For nonresonant scattering it is convenient to use the linear σ- and π-polarization basis. It is assumed that the medium is not optically active, so there is no orthogonal scattering $\hat{\epsilon}_\pi \rightarrow \hat{\epsilon}_\sigma$, $\hat{\epsilon}_\sigma \rightarrow \hat{\epsilon}_\pi$. This is normally valid for x-ray scattering but is *not valid* for resonant γ-ray optics, which has very strong Faraday-type effects as discussed in paper III.[22]

$$g_1 \equiv g'_1 + ig''_1 = k_0 \phi \beta_1 , \tag{2}$$

where the "refraction factor" is

$$\begin{aligned}\beta_1 \equiv \beta'_1 + i\beta''_1 &= [1 + (n\lambda^2 f_e/\pi\phi^2)]^{1/2} \\ &= [1 - (\phi_c/\phi)^2 + i(\lambda/\phi^2 l_A)]^{1/2} .\end{aligned} \tag{3}$$

Here, n is the atomic density (number of atoms/cm^3) and f_e is the atomic forward scattering amplitude due to electronic scattering,[29]

$$f_e = -(Z + \Delta f')r_0 + i(\sigma_e/4\pi\lambda) . \tag{4}$$

The first term, Zr_0, where Z is the atomic number and $r_0 = e^2/mc^2 = 2.8 \times 10^{-13}$ cm is the classical electron radius, is due to Thomson scattering and gives the dominant real contribution. The second term, $\Delta f' r_0$, is the anomalous scattering contribution, which is only appreciable near or below an absorption edge. Finally, the imaginary contribution gives the effects of absorption. Here, σ_e is the total cross section which in the 10-keV x-ray region is dominated by photoabsorption. In the second line of Eq. (3), ϕ_c is the critical angle,

$$\phi_c=[n\lambda^2 r_0(Z+\Delta f')/\pi]^{1/2}\,, \tag{5}$$

and l_A is the absorption length,

$$l_A=(n\sigma_e)^{-1}\,. \tag{6}$$

For a medium with several atomic species, $nf_e\rightarrow\sum n_j f_j$.

The perpendicular penetration depth of the wave in medium 1 is determined by the imaginary part of g_1,

$$l_\perp(\phi)=(2g_1'')^{-1}=\lambda\!\!\!^{-}/2\phi\beta_1''\,. \tag{7}$$

Applying the boundary conditions on E and B across the surface gives the Fresnel formula for the reflection amplitude,[29]

$$R_{01}(\phi)=\left[\frac{1-\beta_1}{1+\beta_1}\right]=\frac{1-[1-(\phi_c/\phi)^2+i(\lambda\!\!\!^{-}/\phi^2 l_A)]^{1/2}}{1+[1-(\phi_c/\phi)^2+i(\lambda\!\!\!^{-}/\phi^2 l_A)]^{1/2}}\,. \tag{8}$$

Our primary interest is in Mössbauer γ rays and we shall use the 14.4-keV γ ray of ^{57}Fe as our main example. In Fig. 2 we plot the reflectivity $|R_{01}(\phi)|^2$ and the penetration depth $l_\perp(\phi)$ vs ϕ for grazing incidence of 14.4-keV radiation from a flat ^{56}Fe surface. Here, $Z=26$, $\Delta f'=0.27$, and $n=8.5\times10^{22}/\text{cm}^3$, giving a critical angle of $\phi_c=3.8\times10^{-3}$ rad, and the photoelectric absorption cross section is $\sigma_e=6.1\times10^{-21}$ cm^2, giving a photoabsorption length $l_A=1.9\times10^{-3}$ cm.

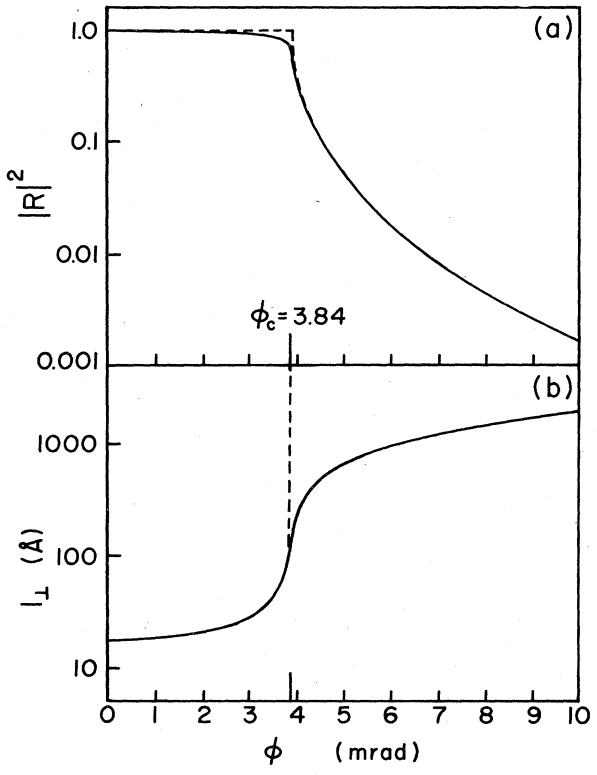

FIG. 2. (a) Reflectivity $|R(\phi)|^2$ vs ϕ and (b) perpendicular penetration depth $l_\perp(\phi)$ vs ϕ for grazing-incidence reflection of 0.86-Å radiation from ^{56}Fe (solid curves). The dashed curves give the hypothetical results in the absence of absorption, $\sigma_e\rightarrow0$.

In the absence of photoabsorption, the reflectivity and penetration depth are shown by the dashed curves in Fig. 2. For $\phi<\phi_c$, β_1 is purely imaginary, $\beta_1=[1-(\phi_c/\phi)^2]^{1/2}=i[(\phi_c/\phi)^2-1]^{1/2}$, and total reflection occurs, $|R_{01}(\phi<\phi_c)|^2=1$. The penetration depth $l_\perp(\phi)=\lambda\!\!\!^{-}/2(\phi_c^2-\phi^2)^{1/2}$, which is very shallow, ≈20 Å over most of the region, but becomes infinite as $\phi\rightarrow\phi_c$. For $\phi>\phi_c$, β_1 is real, the reflectivity falls off asymptotically as $(\phi_c/\phi)^4/16\propto\phi^{-4}$, and the penetration depth is infinite.

The effect of photoabsorption is to decrease the reflectivity, and to limit the penetration depth. Now, as $\phi\rightarrow\phi_c$, $l_\perp\rightarrow(\lambda\!\!\!^{-}l_A/2)^{1/2}=116$ Å, while for $\phi\gg\phi_c$, $l_\perp\approx l_A\phi\approx2.0\phi\times10^5$ Å, which is the usual penetration depth limited by photoabsorption. Although the penetration depth is now limited, $l_\perp$ still becomes very deep for $\phi>\phi_c$, increasing from ≈20 Å for $\phi<\phi_c=3.8$ mrad, to 116 Å at $\phi=\phi_c$, to 472 Å at $\phi=4.5$ mrad. This rapid increase in $l_\perp$ for $\phi>\phi_c$ is necessary for antireflection coatings since the penetration depth must exceed the film thickness.

B. Uniform film coating

For grazing-incidence reflection from a surface coated with a uniform film of thickness l_1, there are transmitted and reflected waves $\exp(\pm ig_1 z)$ in the film and a transmitted wave $\exp(ig_2 z)$ in medium 2, as indicated in Fig. 1(b). Here the complex wave vector $g_j=g_j'+ig_j''=k_0\phi\beta_j$. Applying the boundary conditions at the two interfaces gives the reflection amplitude[18]

$$R(\phi)=\frac{R_{01}+R_{12}e^{i2g_1 l_1}}{1+R_{01}R_{12}e^{i2g_1 l_1}}\,, \tag{9}$$

where R_{01} and R_{12} are the reflection amplitudes at the medium interfaces 0-1 and 1-2, respectively,

$$R_{01}(\phi)=(1-\beta_1)/(1+\beta_1)\,,\qquad R_{12}(\phi)=(\beta_1-\beta_2)/(\beta_1+\beta_2)\,, \tag{10}$$

where for medium j,

$$\beta_j\equiv\beta_j'+i\beta_j''=\{1+[n(j)\lambda^2 f_e(j)/\pi\phi^2]\}^{1/2}=\{1-[\phi_c(j)/\phi]^2+i[\lambda\!\!\!^{-}/\phi^2 l_A(j)]\}^{1/2}\,. \tag{11}$$

C. Multiple layers

For a multilayer media, the reflection amplitude can be obtained by iteration: For a substrate covered with two uniform films, the reflection amplitude is

$$R(\phi)=\frac{R_{01}+e^{i2g_1 l_1}R_{12}^{\dagger}}{1+R_{01}R_{12}^{\dagger}e^{i2g_1 l_1}}\,, \tag{12}$$

where $R_{12}^{\dagger}$ is the compound reflectivity arising at the 1-2 interface (from both film 2 and medium 3), which is given by Eq. (9):

$$R_{12}^{\dagger}=\frac{R_{12}+R_{23}e^{i2g_2l_2}}{1+R_{12}R_{23}e^{i2g_2l_2}} . \tag{13}$$

This iteration procedure can be extended to an arbitrary number of layers, replacing R_{23} by the compound reflectivity $R_{23}^{\dagger}$ in Eq. (13), etc.

An alternative solution can be given in terms of the "characteristic matrices" $\mathscr{M}_n$ which relate the E and B fields at the upper and lower boundaries of the nth film. This is the customary approach used in treating optical reflections from dielectric thin films[1] and the formalism can be taken over directly with minor modifications for the strong x-ray absorption. This approach is summarized in Appendix B.

III. IMPEDANCE-MATCHED λ/4 FILMS AND DAMPING-STABILIZED SOLUTIONS

For an antireflection coating, the wave reflected from the interfaces must be of equal amplitude and emerge 180° out of phase. In this paper we examine the conditions for an antireflection coating when the reflecting mirror is coated with a *single* film of *lower* electron density. In the limit of negligible photoabsorption, antireflection coatings for this case are impedance-matched "quarter-wave" films. When photoabsorption is taken into account, the quarter-wave film conditions are modified and, in addition, there are new "damping-stabilized" solutions which are intermediate between λ/4 and λ/2 films.

A. Limit $\sigma_e \to 0$

For a mirror (2) coated with a single film (1), the reflection amplitude is given by Eq. (9). Assuming the film has lower electron density, then $\phi_{c1}<\phi_{c2}$, and in the region $\phi>\phi_{c2}$, R_{01}, R_{12}, and g_1 are purely real when $\sigma_e(1)=\sigma_e(2)=0$.

The impedance-match condition $R_{01}=R_{12}$ reduces to $\beta_1^2=\beta_2$, which requires an electron density

$$\rho_1(\phi)\equiv n_1(Z+\Delta f_1') =\rho_2(\phi/\phi_{c2})^2\{1-[1-(\phi_{c2}/\phi)^2]^{1/2}\} , \tag{14}$$

and the destructive interference condition $\exp(i2g_1l_1)=-1$ requires a quarter-wave film: the film thickness should be an *odd multiple* of

$$l_1(\phi)=\lambda/4(\phi^2-\phi_{c1}^2)^{1/2} , \tag{15}$$

which, using Eq. (14) to determine ϕ_{c1}, gives

$$l_1(\phi)=\lambda/4\phi[1-(\phi_{c2}/\phi)^2]^{1/4} \tag{15'}$$

for an impedance-matched quarter-wave film.

Both the required electron density and proper film thickness depend on the angle of incidence ϕ. An examination of Eqs. (14) and (15) shows that the required electron density varies from $\rho_1(\phi)=\rho_2$ at $\phi=\phi_{c2}$ decreasing to $\approx\frac{1}{2}\rho_2$ for $\phi\gg\phi_{c2}$, and the required l_1 decreases from ∞ at $\phi=\phi_{c2}$ to $\lambda/4\phi$ for $\phi\gg\phi_{c2}$. This behavior is shown explicitly in Figs. 3(a) and 3(b) for the case of 14.4-keV radiation incident on a coated Fe mirror. Here,

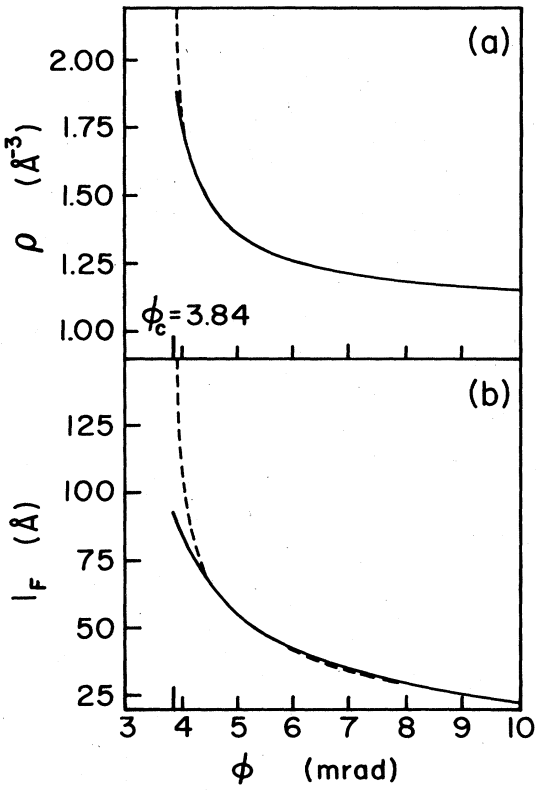

FIG. 3. (a) Required electron density $\rho_1(\phi)$ for an impedance-matched film on an ^{56}Fe mirror reflecting 0.86-Å radiation. The dashed curve is for the hypothetical limit $\sigma_e\to 0$, while the solid curve includes photoabsorption. (b) Required film thickness $l_1(\phi)$ for an impedance-matched quarter-wave film.

$\rho_2=2.24/\text{Å}^3$ and $\phi_{c2}=3.8$ mrad, and we see that the required thickness decreases from ≈ 87 Å at $\phi=4.0$ mrad to ≈ 25 Å at $\phi=10$ mrad.

For a coating of given ρ_1, Eq. (14) determines the angle ϕ_0 at which an impedance match occurs,

$$\phi_0=(\rho_1/\rho_2)^{1/2}\phi_{c2}/(2-\rho_2/\rho_1)^{1/2} , \tag{16}$$

and for a quarter-wave film, the thickness should be taken as $l_1(\phi_0)$ as determined by Eq. (15).

For an ^{56}Fe mirror ($\rho_2=2.24$ Å^{-3}), there are many possible coatings with $\frac{1}{2}\rho_2<\rho_1<\rho_2$. Table I gives the op-

TABLE I. Optimal parameters l_1,ϕ_0 for several coatings on Fe, reflecting 14.4-keV radiation in the limit $\sigma_e\to 0$.

	ρ_1/ρ_2	ϕ_0 (mrad)	l_1 (Å)
Ti	0.55	6.30	38.4
Se	0.56	6.26	38.7
Ge	0.64	4.68	60.9
Te	0.69	4.31	74.4
Ga	0.71	4.21	80.3
V	0.74	4.14	85.2
Sb	0.76	4.05	95.2
Ce	0.76	4.04	96.6
Zr	0.77	4.02	99.6

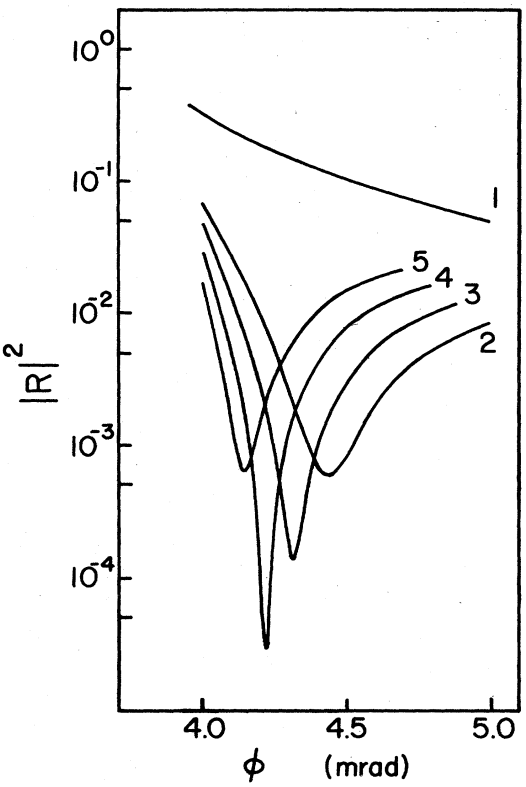

FIG. 4. $|R|^2$ vs ϕ for ^{56}Fe coated with (1) uncoated, (2) 70-Å Te, (3) 75-Å Te, (4) 80-Å Te, and (5) 85-Å Te.

timum parameters $\phi_0, l_1(\phi_0)$ determined from Eqs. (15) and (16) for several possible impedance-matched quarter-wave films on Fe for 14.4-keV radiation. In these cases the optimal parameters range from $l_1=38$ Å, $\phi_0=6.3$ mrad for Ti to $l_1=100$ Å, $\phi_0=4.0$ mrad for the higher-density Zr coat.

Figure 4 shows rocking curves $|R|^2$ vs ϕ for different thicknesses of Te on Fe, where, here, photoabsorption is taken into account. We note the position $\phi_{\min}$ of minimum reflectivity changes with thickness due to the changing quarter-wave condition. There is an optimal thickness $l_1 \approx 80$ Å and an optimal angle of incidence $\phi_0 \approx 4.2$ mrad for maximum suppression. These optimal parameters are close to the estimate of Eqs. (15) and (16) given in Table I but are appreciably shifted by the effects of photoabsorption. Of course, the most interesting feature of Fig. 4 is that very significant suppression occurs, with the reflectivity reduced by 3–4 orders of magnitude.

B. General treatment for $\sigma_e \neq 0$

In the limit $\sigma_e \to 0$ discussed above, the antireflection coating is restricted to an electron density $\frac{1}{2}\rho_2 \leq \rho_1 \leq \rho_2$ and reflection must occur in the region $\phi > \phi_{c2}$ $(> \phi_{c1})$. For $\sigma_e \neq 0$, there are significant shifts in the optimum parameters ϕ_0, l_1 for a quarter-wave-film antireflection coating, and there is a new set of damping-stabilized solutions for antireflection coatings in the previously inaccessible region $\phi_{c1} < \phi < \phi_{c2}$, which also allow low-density coatings $\rho_1 < \frac{1}{2}\rho_2$.

To treat the general case, we rewrite the reflection amplitude Eq. (9) as

$$R(\phi) = \frac{r_{01}e^{i\phi_{01}} + r_{12}e^{-2g_1''l_1}e^{i(\phi_{12}+2g_1'l_1)}}{1+R_{01}R_{12}e^{i2g_1l_1}}, \tag{17}$$

where we have introduced the amplitudes and phases of the interface reflection amplitudes,

$$\begin{aligned} R_{01}(\phi) &= r_{01}(\phi)e^{i\phi_{01}(\phi)}, \\ R_{12}(\phi) &= r_{12}(\phi)e^{i\phi_{12}(\phi)}, \end{aligned} \tag{18}$$

and, as before, g_1' and g_1'' are the real and imaginary parts of the complex wave vector.

The behavior of the separate interface reflection amplitudes and phases are shown in Fig. 5 for $\sigma_e=0$ and in Fig. 6 for $\sigma_e \neq 0$, again for Te on Fe reflecting 14.4-keV radiation: In Fig. 5(a) the solid curve gives $r_{01}(\phi)$, the magnitude of the reflection amplitude from the top film surface, while the dotted curve gives $r_{12}(\phi) \times \exp[-2g_1''(\phi)l_1]$, the magnitude of the wave amplitude reflected from the film-mirror interface, including the extinction effects of propagating through the film. Since here $\sigma_e=0$, then $g_1''(\phi)=0$ for $\phi > \phi_{c1}$ and in this region the dotted curve coincides with $r_{12}(\phi)$. However, for $\phi < \phi_{c1}$, there is strong primary extinction ($g_1'' \neq 0$), so the reflected amplitude depends on the film thickness l_1 and is strongly reduced from r_{12}. [In the region $\phi < \phi_{c1}$, the dashed curve gives $r_{12}(\phi)$.] Now, $r_{01}(\phi)$ is just the usual grazing-incidence reflection amplitude from a single surface and exhibits the features discussed in Sec. II A: Total reflection occurs for $\phi < \phi_{c1}$ (where β_1 is imaginary), rapidly decreasing $\sim \phi_{c1}^2/4\phi^2$ for $\phi > \phi_{c1}$ (where β_1 is real). On the other hand, $r_{12}(\phi)$ only exhibits total reflection in

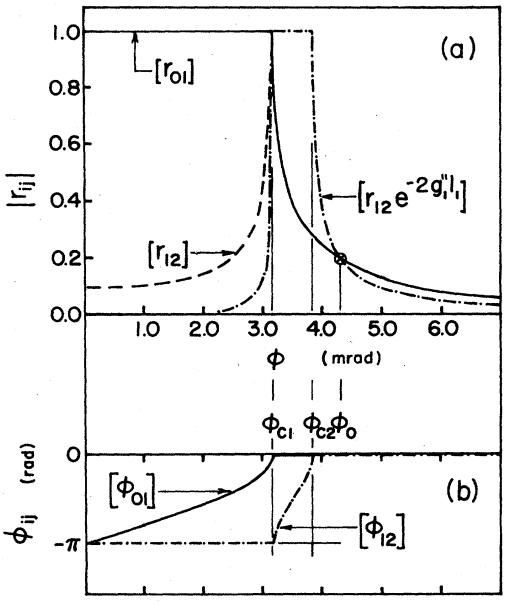

FIG. 5. (a) Interface reflection amplitudes vs ϕ and (b) phases of the interface reflections vs ϕ for 80-Å Te on Fe ($\sigma_e=0$).

the region $\phi_{c1} \lesssim \phi \lesssim \phi_{c2}$ (where β_1 is real and β_2 imaginary) and falls off rapidly $\sim(\phi_{c2}^2-\phi_{c1}^2)/4\phi^2$ for $\phi > \phi_{c2}$ (where both β_1 and β_2 are real) and for $\phi < \phi_{c1}$ (where both β_1 and β_2 are imaginary). In the latter region,

$$r_{12}(\phi) \rightarrow (\phi_{c2}-\phi_{c1})/(\phi_{c2}+\phi_{c1})$$

as $\phi \rightarrow 0$.

Figure 6(a) includes the effects of photoabsorption. The solid curve again gives $r_{01}(\phi)$ and the dotted curve gives $r_{12}(\phi)\exp(-2g_1''l_1)$. However, now $g_1'' \neq 0$ for all ϕ, so the effective reflection amplitude of the film-mirror interface depends explicitly on the film thickness for all ϕ. Here the curves are calculated for 80 Å of Te on ^{56}Fe. The primary effect of photoabsorption is to reduce the reflection amplitudes somewhat and produces a general "degradation" of the curves.

Figures 5(b) and 6(b) give the phases of the reflection amplitudes for $\sigma_e = 0$ and $\sigma_e \neq 0$, respectively. In both cases, the solid curve gives $\phi_{01}(\phi)$ (the phase of the reflection from the 0-1 interface) and the dashed curve gives $\phi_{12}(\phi)$ (the phase of the 1-2 interface reflection). We see in Fig. 5(b) that in the absence of photoabsorption, the two phases vary rapidly in the corresponding total-reflection regions of r_{01} and r_{12}, with ϕ_{01} increasing from $-\pi \rightarrow 0$ as $\phi \propto 0 \rightarrow \phi_{c1}$ and with ϕ_{12} increasing from $-\pi \rightarrow 0$ as $\phi \propto \phi_{c1} \rightarrow \phi_{c2}$, and that outside these regions, the phases remain constant. Again photoabsorption gives a small degradation of the curves as shown in Fig. 6(b).

The rapid variation of the phases is reminiscent of the rapid phase variation in the region of total Bragg reflection. This of course is not coincidental: From the point of view of the dynamical theory,[26,27] grazing-incidence reflection from a single surface can be viewed as a zero-angle Bragg reflection, with the region of total Bragg reflection being $0 \lesssim \phi \lesssim \phi_c$. The dynamical treatment is discussed in Appendix A. We now return to the total reflection amplitude of Eq. (17) and examine the general conditions for an antireflection coating.

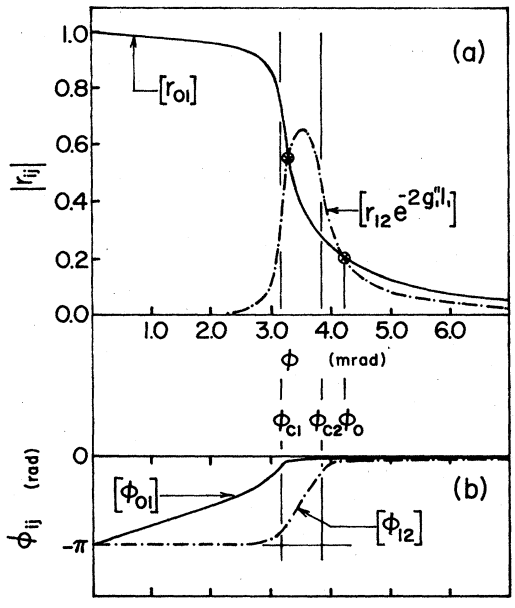

FIG. 6. Interface reflection amplitudes and phases vs ϕ for 80-Å Te on Fe at 14.4 keV ($\sigma_e \neq 0$).

1. Impedance match

The general impedance-match condition is

$$r_{01}(\phi) = r_{12}(\phi)e^{-2g_1''(\phi)l_1} . \tag{19}$$

In the limit of no photoabsorption, $g_1''(\phi) = 0$ (for $\phi > \phi_{c1}$) and the impedance-match condition then determines a unique electron density $\rho_1(\phi)$, as given by Eq. (14), which produces an impedance match at the angle ϕ. Alternatively, the impedance-match condition determines the angle ϕ_0 at which exact impedance match occurs. In Fig. 5(a) ϕ_0 is determined by the intersection of the curves for $r_{01}(\phi)$ and $r_{12}(\phi)$ in the region $\phi > \phi_2$. An intersection for impedance match also occurs at $\phi_0' = \phi_{c1}$, where total reflection occurs at both interfaces. In this limit ($\sigma_e = 0$), the intersections ϕ_0, ϕ_0' are independent of the film thickness l_1.

However, when photoabsorption is included, the impedance-match condition, Eq. (19), depends on the film thickness l_1 as well as ϕ, which has the following effect: For a given l_1, if an exact match occurs at the angle ϕ_0, i.e.,

$$r_{01}(\phi_0) = r_{12}(\phi_0)\exp[-2g_1''(\phi_0)l_1] ,$$

a change in film thickness will cause a mismatch. Thus, photoabsorption causes the impedance-match angle ϕ_0 to be dependent on l_1 and now, rather than a single ϕ_0 (with arbitrary thickness), there is a region of impedance-match angles $\phi_0(l_1)$ and a range of film thickness l_1 for which it is possible to achieve an impedance match.

Figure 7(a) gives the curves for $r_{01}(\phi)$ and $r_{12}(\phi)\exp(-2g_1''l_1)$ for various film thickness l_1 (Te on Fe, $E_\gamma = 14.4$ keV). From these curves, it is clear that due to photoextinction of the lower reflection there is a maximum thickness l_1^* beyond which no impedance match is possible. For any $l_1 < l_1^*$, there are two intersections: $\phi_0(l_1)$ which lies in the region $\phi_{c2} \lesssim \phi_0(l_1) < \phi_0$ and decreases with increasing l_1, and $\phi_0'(l_1)$ which lies in the region $\phi_{c1} < \phi_0'(l_1) \lesssim \phi_{c2}$ and increases with increasing l_1.

From the impedance-match condition, Eq. (19), we can solve for $l_1^{(=)}(\phi)$, the film thickness which gives an exact impedance match at the angle ϕ,

$$l_1^{(=)}(\phi) = l_\perp^{(1)}(\phi)\ln[r_{12}(\phi)/r_{01}(\phi)] , \tag{20}$$

where, as defined in Eq. (7), $l_\perp^{(1)}(\phi) = [2g_1''(\phi)]^{-1}$ gives the maximum perpendicular penetration depth permitted in the film medium for a wave incident at the angle ϕ. We note that Eq. (20) requires $r_{12} > r_{01}$, i.e., the reflection at the second interface must be stronger than the reflection from the first interface, which of course is necessary to offset the absorption in propagating through film 1.

The solid line in Fig. 7(b) gives $l_1^{(=)}(\phi)$ for Te on Fe and $E_\gamma = 14.4$ keV. For this case it is possible to find film thicknesses satisfying the impedance-match condition in the region $\phi_{c1} = 3.1$ mrad to $\phi_0 = 4.3$ mrad, with the maximum possible thickness being $l_1^* = 490$ Å at

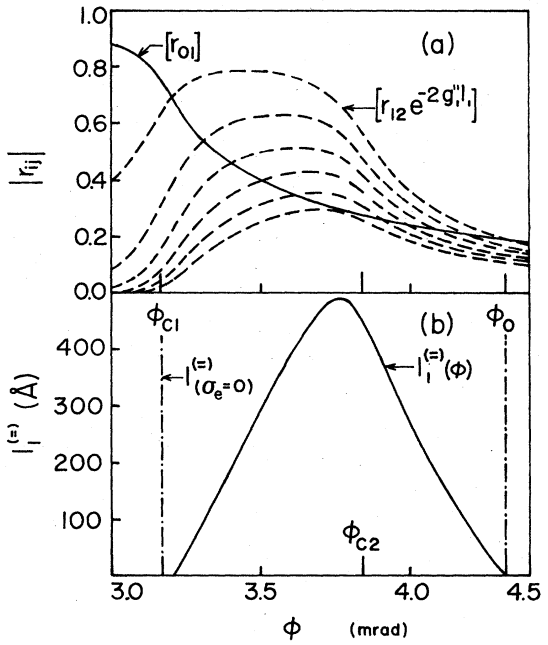

FIG. 7. (a) Lower interface reflection amplitude $r_{12}(\phi)\exp[-2g_1''(\phi)l_1]$ vs ϕ for $l_1=0, 100, \ldots, 500$ Å (dashed curves) and upper interface $r_{01}(\phi)$ vs ϕ (solid curve) for Te on Fe at 14.4 keV. (b) Required film thickness $l_1^{(=)}(\phi)$ for exact impedance match at angle ϕ. Dashed line gives limiting case of $\sigma_e=0$.

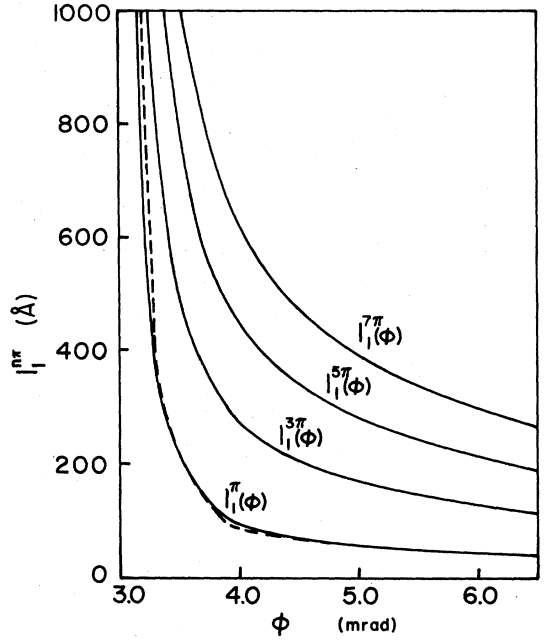

FIG. 8. Required film thickness $l_1^{m\pi}(\phi)$ to produce an $m\pi$ relative phase shift of lower reflection at angle ϕ for $m=1$, 3, 5, and 7, for Te on Fe at 14.4 keV.

$\phi=3.8$ mrad$\simeq\phi_{c2}$. The dashed line in Fig. 7(b) gives the limiting case of $\sigma_e=0$. In this limit, impedance match occurs for *any* thickness at ϕ_{c1} and at ϕ_0, giving vertical dashed lines for $l_1^{(=)}$ at these two angles.

2. *Destructive interference*

Returning to Eq. (17), the condition for destructive interference is

$$\exp\{i[\phi_{12}(\phi)+2g_1'(\phi)l_1-\phi_{01}(\phi)]\}=-1\ , \tag{21}$$

which requires the phase to be $m\pi$, m being *odd*. The corresponding film thickness $l_1^{m\pi}(\phi)$ which gives such a relative phase shift to the reflected waves (when the incidence angle is ϕ) is

$$l_1^{m\pi}(\phi)=[m\pi-\phi_{12}(\phi)+\phi_{01}(\phi)]/2g_1'(\phi)\ . \tag{22}$$

The required film thickness decreases with increasing ϕ because the phase change only involves the z component of the refracted wave g_1' which increases with ϕ (for $\phi>\phi_{c1}$, $[2g_1'(\phi)]^{-1}\simeq\lambda/4\pi(\phi^2-\phi_{c1}^2)^{1/2}$). Furthermore, for low-density coatings ($\rho_1<\rho_2$) and $\phi>\phi_{c2}$, $\phi_{12}(\phi)=\phi_{01}(\phi)=0$, as shown in Figs. 5(b) and 6(b), and Eq. (22), gives the quarter-wave-film thickness discussed earlier, $l_1^{m\pi}\simeq m[\lambda/4(\phi^2-\phi_{c1}^2)^{1/2}]$. However, for $\phi_{c1}\lesssim\phi\lesssim\phi_{c2}$, $\phi_{12}(\phi)$ varies rapidly from $-\pi$ to 0, while $\phi_{01}(\phi)\simeq 0$ and the required film thickness is intermediate between a quarter- to a half-wave film.

In Fig. 8 the $l_1^{m\pi}(\phi)$ curves are given for $m=1$, 3, 5, and 7 for Te on Fe and 14.4 keV. The dashed curve gives the limit $\sigma_e\to 0$, while the solid curves include photoabsorption.

3. *Antireflection coatings*

The intersections of $l_1^{(=)}(\phi)$ with the curves $l_1^{m\pi}(\phi)$ determine the required film thicknesses and angles of incidence for impedance-matched antireflection coatings which will strongly suppress x-ray scattering.

Figure 9(a) shows the limit $\sigma_e=0$ for Te on Fe. Here, $l_1^{(=)}(\phi)$ is two vertical lines at $\phi_{c1}=3.1$ mrad and $\phi_0=4.3$ mrad, and since all the curves $l_1^{m\pi}(\phi)\to\infty$ as ϕ decreases to ϕ_{c1}, intersections only occur at ϕ_0. These are simply the quarter-wave films discussed earlier: a GIAR coating requires 73 Å of Te on Fe and all other possible coatings are odd multiples of this thickness.

In contrast, when photoabsorption is taken into account as in Fig. 9(b), there are only a finite number of possible coatings, the thickness and operating angles are strongly shifted, and a new set of damping-stabilized solutions appear: Due to photoabsorption, the impedance-match curve $l_1^{(=)}(\phi)$ is now deformed from two parallel lines to a bell-shaped curve in the region $\phi_{c1}\lesssim\phi\lesssim\phi_0$, with maximum near ϕ_{c2}. The π-phase curves $l_1^{m\pi}(\phi)$ monotonically decrease in this region and each curve that intersects $l_1^{(=)}(\phi)$ will have two intersections—one at $\phi_0(m\pi)$ in the region $\phi_{c2}\lesssim\phi<\phi_0$ with thickness $l_1(m\pi)$, and one at $\phi_0'(m\pi)$ in the region $\phi_{c1}<\phi\lesssim\phi_{c2}$ with thickness $l_1'(m\pi)$.

The antireflection coatings $l_1(m\pi)$, which have operating angles $\phi_0(m\pi)$ in the region $\phi_{c2}\to\phi_0$, are quarter-wave films, but with significant shifts in the parameters from the $\sigma_e=0$ limit. The operating angle $\phi_0(m\pi)$ is decreased from ϕ_0 and correspondingly the appropriate thickness

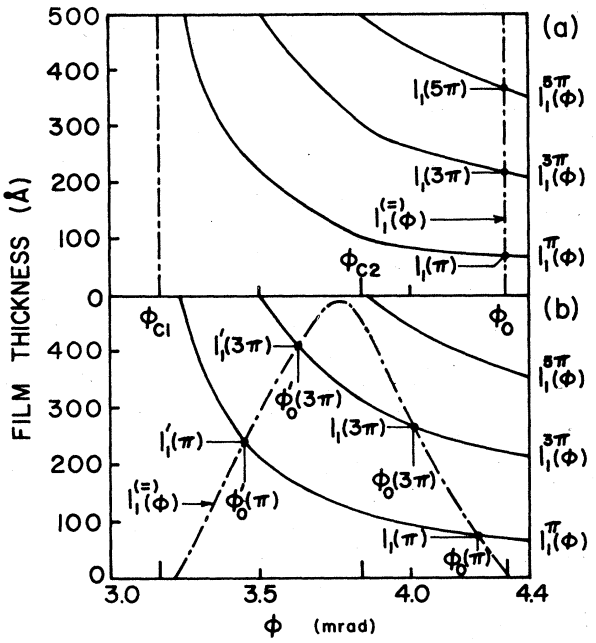

FIG. 9. Graphical solution for the film thickness $l_1(m\pi)$ and operating angle $\phi_0(m\pi)$ required for an antireflective film. (a) gives the limit $\sigma_e=0$. In (b), the new intersections $l_1'(m\pi),\phi_0'(m\pi)$ give the damping-stabilized solutions.

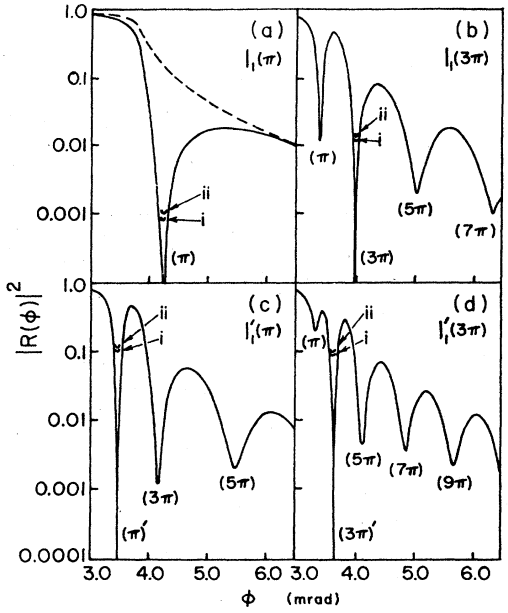

FIG. 10. Rocking curves $|R|^2$ vs ϕ for reflection of 14.4-keV radiation from the four possible GIAR films of Te on Fe. The two curves (i and ii) at the principal minima give the reflectivity averaged over an incident beam spread of $\Delta\phi=0.2$ mrad and a double average over beam spread and a long-range film thickness variation $l_1\pm0.025l_1$.

$l_1(m\pi)$ is increased. Also, $l_1(m\pi)$ is no longer a simple multiple of $l_1(\pi)$.

The new solutions $l_1'(m\pi)$, which have operating angles $\phi_0'(m\pi)$, in the region $\phi_{c1}\rightarrow\phi_{c2}$, are only possible due to photoabsorption and will be referred to as damping-stabilized solutions. They have a simple origin: In the absence of photoabsorption there is total reflection from the lower surface 2 for $\phi_{c1}\leq\phi\leq\phi_{c2}$ and a weaker reflection from the upper surface 1, so exact cancellation is never possible. With photoabsorption, extinction occurs in film 1 which reduces the reflected wave from 2, with the reduction being stronger as ϕ decreases to ϕ_{c1} due to the increased path length of the wave in the film. Therefore, as $\phi\rightarrow\phi_{c1}$, there will always be an angle $\phi_{(=)}'$ at which the two reflected waves are equal in magnitude, and by appropriate choice of thickness, phase cancellation will occur.

Because $l_1^{m\pi}(\phi)$ monotonically decreases, the damping-stabilized GIAR film will always be thicker than the corresponding $\lambda/4$ film, i.e., $l_1'(m\pi)>l_1(m\pi)$. Also, because of the rapid variation of the phase $\phi_{12}(\phi)$ in the region $\phi_{c1}\leq\phi\leq\phi_{c2}$, $l_1'(m\pi)$ will be intermediate between a quarter- to a half-wave film.

The parameters obtained from Fig. 9 for the possible GIAR films of Te on Fe are tabulated in Table II, and Fig. 10 gives the rocking curves $|R(\phi)|^2$ vs incidence angle ϕ for each of the possible film thicknesses, $l_1=l_1(m\pi)$ or $l_1'(m\pi)$. In each case, a very deep minimum occurs at the angle $\phi_0(m\pi)$ or $\phi_0'(m\pi)$ for which an impedance-matched antireflection condition holds. The additional minima occur at those angles at which the film gives any odd-order π-phase shift to the lower reflection, i.e., at ϕ such that $l_1^{m\pi}(\phi)=l_1$, which can be determined graphically from Fig. 8. Although there is no impedance match for these subsidiary minima, they are still quite pronounced, particularly at larger angles $\phi\gtrsim\phi_0$, where the difference $[r_{01}-r_{12}\exp(-2g_1''l_1)]$ is small [see Figs. 6(a) and 7(a)].

C. Beam divergence and film-thickness variations

Two obvious factors limit the degree of suppression: (1) the divergence of the incident beam (or equivalently, the long-range variation of the local surface normal) and (2) the long-range variation of the thickness of the film. The

TABLE II. Parameters for the possible GIAR films of Te on Fe for reflection of 14.4-keV radiation.

$\sigma_e=0$		$\sigma_e\neq0$				
$\phi_0(m\pi)$ (mrad)	$l_1(m\pi)$ (Å)	$\phi_0(m\pi)$ (mrad)	$l_1(m\pi)$ (Å)	$\phi_0'(m\pi)$ (mrad)	$l_1'(m\pi)$ (Å)	m
4.32	73	4.22	80	3.45	240	1
4.32	219	4.01	268	3.63	409	3
4.32	365					5

much more fundamental question of the effect of the microscopic "surface roughness" is discussed in paper VI.[25]

For the synchrotron source DORIS, the vertical divergence of the x-ray beam at 10 keV is ≈ 0.1–0.2 mrad.[30] The long-range thickness control in producing thin films is about 5% absolute thickness.[31]

For a $\lambda/4$-GIAR film $[\phi_0(m\pi) > \phi_{c2}]$, one main effect of beam divergence and film thickness variations is a change of the quarter-wave condition. Neglecting photoabsorption, if a film of thickness l_1 is a quarter-wave film for a wave incident at ϕ_0, then the phase change for propagation through the film is

$$2l\phi_0[1-(\phi_{c1}/\phi_0)^2]^{1/2}/\lambda = m\pi \ .$$

For film $l' = l + \Delta l$ and a wave incident at $\phi = \phi_0 + \Delta\phi$,

$$2l_1'\phi[1-(\phi_{c1}/\phi)^2]^{1/2}\lambda = m\pi + \epsilon \ , \tag{23}$$

where $\epsilon = \epsilon(\Delta\phi) + \epsilon(\Delta l)$,

$$\epsilon(\Delta\phi) = \frac{\Delta\phi}{\phi_0} m\pi\phi_0^2/(\phi_0^2 - \phi_{c1}^2) \ ,$$
$$\epsilon(\Delta l) = \frac{\Delta l}{l_1} m\pi \ . \tag{23'}$$

Assuming the film is also impedance matched so that $r_{01} = r_{12}$ at ϕ_0, then at $\phi_0 + \Delta\phi$ and $l_1 + \Delta l$,

$$|R|^2 \approx |R_{01} + R_{12} e^{i2l_1'g_1}|^2 \approx |r_{01}|^2 \epsilon^2 \ . \tag{24}$$

For a beam divergence of 0.2 mrad and thickness control to $\Delta l/l_1 = \pm 0.025$, $|\epsilon| \lesssim 0.2$ and $|R|^2 \lesssim 0.04\,|r_{01}|^2$ (for the lowest-order film $m=1$). At an angle where the uncoated medium 2 would have $\approx 10\%$ reflectivity, i.e., $r_{02} \approx 0.3$, the impedance-matched coated medium will have reduced reflectivities at each interface, typically $r_{01} \approx r_{12} \approx 0.15$, so that the coated medium will typically have a reflectivity $|R|^2 \lesssim 10^{-3}$ over the entire divergence and thickness variation of the film. These effects will be more severe for the higher-order films.

A second effect, which we have neglected above, is the variation of the reflection amplitudes with ϕ: Even with an exact impedance match at ϕ_0, i.e., $r_{01}(\phi_0) = r_{12}(\phi_0)$, there will be a mismatch at $\phi_0 + \Delta\phi$,

$$r_{01}(\phi_0+\Delta\phi) - r_{12}(\phi_0+\Delta\phi) \simeq (dr_{01}/d\phi - dr_{12}/d\phi)\Delta\phi \ .$$

For $\lambda/4$-GIAR films $[\phi_0(m\pi) > \phi_{c2}]$, both amplitudes have negative slope and are already small ($\lesssim 0.1$), so that the difference remains small over a fairly broad angular region. For the 80-Å $\lambda/4$-GIAR film of Te on Fe, $|r_{01} - r_{12}\exp(-2g_1''l_1)|^2$ remains $\lesssim 10^{-3}$ over an angular region $\Delta\phi = 0.46$ mrad about ϕ_0, as shown in Fig. 11. This is about the same order effect as that produced by the phase variation and, taken together, the reflectivity will typically be $|R|^2 \lesssim 10^{-3}$ over a $\Delta\phi \simeq 0.2$–0.3 mrad.

These estimates are modified for damping-stabilized GIAR film ($\phi_{c1} < \phi_0' < \phi_{c2}$) leading to a much more rapid $\Delta\phi$ variation but less sensitivity to Δl variations: First, there is now a rapid impedance mismatch with $\Delta\phi$ because r_{01} and r_{12} are larger and have opposite slopes at ϕ_0'. [For the example of the 240-Å GIAR film of Te on Fe in Fig. 11, $|r_{01} - r_{12}\exp(-2g_1''l_1)|^2 \lesssim 10^{-3}$ only over $\Delta\phi = 0.06$ mrad about ϕ_0'.] Second, the phase change due to film 1 is now

$$2l_1\phi_0'[1-(\phi_{c1}/\phi_0')^2]^{1/2}/\lambda + \phi_{12} = m\pi \ ,$$

so that $\epsilon = \epsilon'(\Delta\phi) + \epsilon(\Delta l)$, where

$$\epsilon'(\Delta\phi) = \Delta\phi\{2l_1/\lambda[1-(\phi_{c1}/\phi_0')^2]^{1/2} + d\phi_{12}(\phi_0')/d\phi\} \ , \tag{23''}$$

and where $\epsilon(\Delta l)$ is still given by Eq. (23'). The variation of $\epsilon'(\Delta\phi)$ with $\Delta\phi$ is now much sharper because $\phi_0' \sim \phi_{c1}$, leading to a large first contribution (the $\hat{z}$ component of the refracted wave vector g_1' rapidly increases for $\phi \gtrsim \phi_{c1}$), and because the additional phase contribution $\phi_{12}(\phi)$ rapidly increases from $-\pi \to 0$ as $\phi \propto \phi_{c1} \to \phi_{c2}$. However, since the damping-stablized film is thicker than the corresponding $\lambda/4$ film, $\epsilon(\Delta l)$ is smaller, so damping-stabilized films are less sensitive to film thickness variations.

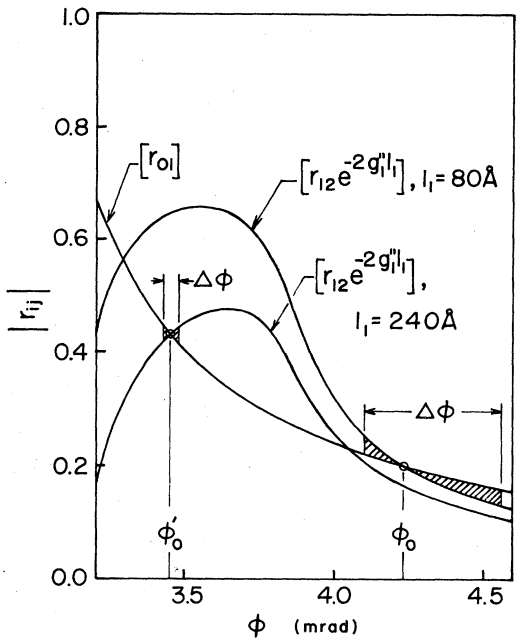

FIG. 11. Interface reflection amplitudes $r_{01}(\phi)$ and $r_{12}(\phi)\exp[-2g_1''(\phi)l_1]$ vs ϕ for Te films on Fe at 14.4 keV for $l_1 = 80$ and 240 Å. Shaded areas show regions over which $|r_{01} - r_{12}\exp(-2g_1''l_1)|^2 \lesssim 10^{-3}$.

The effects of beam divergence and long-range thickness variations are shown in Fig. 10 for the various GIAR films of Te on Fe. Here the solid curves give the rocking curves $|R|^2$ vs ϕ for the idealized cases of $\Delta\phi = \Delta l = 0$, while the dashed curves near the principal minimum are calculated for a beam spread of $\Delta\phi = 0.2$ mrad and a 5% thickness variation. We note that the damping-stabilized minima and the $3\lambda/4$ minimum are strongly affected, now being only $|R|^2 \approx 10^{-2} - 10^{-1}$, while the $\lambda/4$ minimum is still quite pronounced, $|R|^2 \approx 8 \times 10^{-4}$.

In Table III we give average reflectivities for several

TABLE III. Optimal parameters l_1,ϕ_0 and minimum reflectivities for several coatings on Fe reflecting 14.4-keV radiation. The response is averaged over an incident beam spread of 0.25 mrad and over a long-range film thickness variation of $l_1\pm0.025l_1$.

	ϕ_0 (mrad)	l_1 (Å)	$\lvert R\rvert^{2\,a}$	$\lvert R\rvert^2_{Fe}/\lvert R\rvert^2$
Ti	6.02	42	2.4(−5)	719
Se	6.03	40	2.1(−5)	807
Ge	4.57	65	3.7(−4)	245
Te	4.38	76	9.4(−4)	135
Ga	4.21	85	2.7(−3)	68
V	4.19	93	3.5(−3)	54
Sb	4.15	97	5.2(−3)	41
Ce	4.12	98	7.2(−3)	32
Zr	4.17	96	4.7(−3)	40

[a]The notation $(-x)$ denotes $\times10^{-x}$.

λ/4-GIAR films on Fe, averaged over a beam divergence of 0.25 mrad and over a variation in film thickness $l_1\pm0.025l_1$. (The optimal parameters l_1,ϕ_0 are shifted somewhat by finite $\Delta\phi,\Delta l$ averages.) We note in particular that strong suppressions are still possible, with, e.g., reduction factors $\lvert R\rvert^2/\lvert R\rvert^2_{Fe}$ of $\frac{1}{807}$ for Se, $\frac{1}{245}$ for Ge, and $\frac{1}{135}$ for Te, corresponding to minimum reflectivities in the range $\lvert R\rvert^2\simeq10^{-5}-10^{-3}$.

D. Frequency range of suppression

For incident "white" synchrotron radiation, an important question is the frequency region over which suppression occurs. For λ/4-GIAR films, one effect of a frequency variation is again the change of the quarter-wave condition, due both to the direct change in λ and to the altered refraction angle (produced by the change in critical angle ϕ_{c1}, which is linear in λ). For a film which is a λ/4-GIAR film for the parameters λ_0,l_1,ϕ_0, a wavelength variation $\lambda_0\rightarrow\lambda_0+\Delta\lambda$ changes the phase to

$$2l_1\phi_0[1-(\phi_{c1}/\phi_0)^2]^{1/2}/\lambda=m\pi+\epsilon(\Delta\lambda)\ ,$$

where

$$\epsilon(\Delta\lambda)=-\frac{\Delta\lambda}{\lambda_0}(m\pi\{1+\phi_{c1}(\lambda_0)^2/[\phi_0^2-\phi_{c1}(\lambda_0)^2]\})\ . \quad (25)$$

As before, for $\lvert\epsilon(\Delta\lambda)\rvert\lesssim0.2$, there is very strong suppression, typically $\lvert R\rvert^2\lesssim10^{-3}$. For the 80-Å GIAR film of Te on Fe, $\lvert\epsilon(\Delta\lambda)\rvert\lesssim0.2$ for $\lvert\Delta\lambda\rvert/\lambda_0\lesssim0.04$, which corresponds to 14.4 keV±600 eV.

A frequency variation also effects the impedance-match condition because the critical angles ϕ_{c1},ϕ_{c2} are changed as $\lambda_0\rightarrow\lambda_0+\Delta\lambda$, which changes the reflectivities r_{01} and r_{12}. Because ϕ_c is linear in λ [Eq. (5)], the resulting mismatch is very nearly that produced by an effective angular variation $\Delta\phi=(\Delta\lambda/\lambda_0)\phi_c$. For the 80-Å Te GIAR film, $\lvert r_{01}-r_{12}\exp(-2g_1''l_1)\rvert^2\lesssim10^{-3}$ over an angular region $\Delta\phi\simeq0.4$ mrad, which corresponds to a wavelength variation $\Delta\lambda/\lambda_0\simeq\Delta\phi/\phi_c\simeq0.1$, again about 1 keV wide.

The conclusion then is that a λ/4-GIAR film (lowest order) will give a strong suppression to reflection over about a 10% bandwidth, corresponding to ≈1 keV in the 10-keV region. For higher-order films the band will be narrower. Figures 12(a) and 12(b) give $\lvert R\rvert^2$ vs ω for the 80- and 268-Å λ/4-GIAR films of Te on Fe. Here, $\lvert R\rvert^2<10^{-3}$ over the regions $\Delta\omega\approx730$ and 200 eV, respectively.

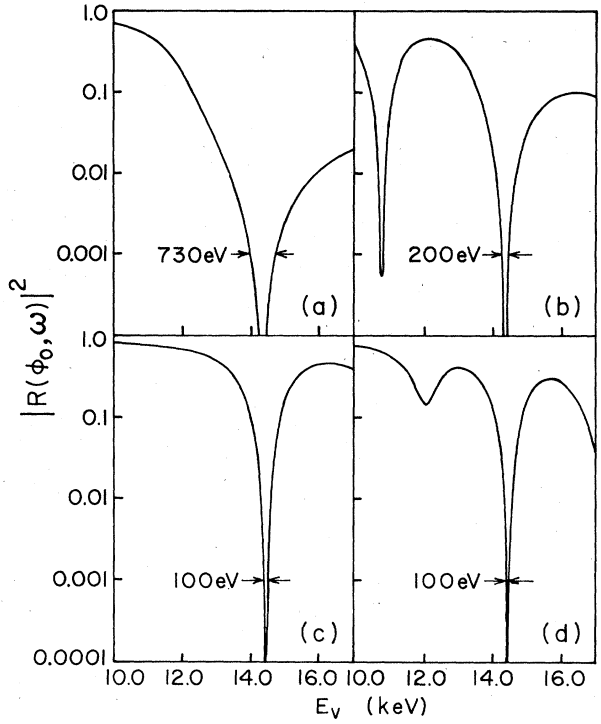

FIG. 12. $\lvert R\rvert^2$ vs ω for the four possible GIAR films of Te on Fe.

For the damping-stabilized film, on the other hand, the phase and impedance-match conditions will vary much more rapidly as $\lambda_0\rightarrow\lambda_0+\Delta\lambda$, just as for angular variations and consequently the frequency region of strong suppression will be narrowed. This is shown explicitly in Figs. 12(c) and 12(d) for the 240- and 409-Å damping-stabilized GIAR films of Te on Fe. However, for $\lvert R\rvert^2\lesssim0.05$, which is a typical reflectivity from a damping-stabilized GIAR film when averaged over thickness variations and beam divergence, $\Delta\omega\approx600$ eV.

IV. SUMMARY

The purpose of this paper has been to develop the basic theory and to examine the simplest techniques for producing grazing-incidence antireflection films to suppress the reflection of 1-Å x rays and to examine the general response of the films—the degree of suppression, the frequency range of suppression, and the limitations imposed by beam divergence and long-range variations in film thickness. Our main conclusions are as follows.

For a mirror coated with a *single film,* there are two possible antireflection coatings—a *λ/4-GIAR film* $(\phi_0>\phi_{c2})$ or a *damping-stabilized* GIAR film $(\phi_{c1}<\phi_0<\phi_{c2})$. In either case the electron density ρ_1 of the film must be less than that of the mirror and, for a given $\rho_1<\rho_2$, the required film thickness l_1 and the

operating angle ϕ_0 for a GIAR film are then uniquely defined.

For a $\lambda/4$-GIAR film, significant changes in the reflectivity occur for angular variations of $\Delta\phi \sim 0.1\phi_c \sim 10^{-4}$ rad and for film thickness variations of $\Delta l \sim 0.1\lambda/\phi \sim 10$ Å. When the response is averaged over long-range variations in film thickness of $\Delta l \approx 10$ Å and angular variations of $\Delta\phi \approx 10^{-4}$ rad, reduced reflectivities of order $10^{-4} \lesssim |R|^2 \lesssim 10^{-3}$ should be possible over about a $\Delta\omega \approx 1$-keV frequency range. For damping-stabilized GIAR films, the angular response is sharper but there is a greater Δl tolerance, giving averaged reflectivities of order $10^{-2} \lesssim |R|^2 \lesssim 10^{-1}$ over a $\Delta\omega \approx 0.5$-keV range.

ACKNOWLEDGMENTS

This work was partially supported by the National Science Foundation Grant No. DMR-80-15706, and the Deutsche Forschungsgemeinschaft and the Bundesministerium für Forschung und Technologie Grant No. 05269GU.

APPENDIX A

Here we briefly outline the dynamical solution for grazing-incidence reflection of γ rays from a mirror coated with one or more films, and we also comment on the essential equivalence of this approach to the index-of-refraction solution.

γ-ray (or x-ray) optics is a single-photon optics governed by simple multiple-scattering equations of a semiclassical form [Eqs. (50) and (51) of Ref. 27]. From these equations, two equivalent formulations of the dynamical theory are possible—a generalized Darwin-Prins planar solution, or a Laue solution.[32] Here we follow the Darwin-Prins solution.

As discussed in Refs. 26 and 27, grazing incidence can be viewed as a special case of Bragg reflection ($\phi_B = 0$). Conceptually dividing film 1 into M layers of thickness $d = l_1/M \to 0$, the dynamical equations are given as

$$\begin{aligned} \mathbf{T}_m &= e^{ig_0 d}[(1+i\tilde{F}^{tt})\mathbf{T}_{m-1} + i\tilde{F}^{tr}\mathbf{R}_{m-1}] , \\ \mathbf{R}_m &= e^{ig_0 d}[(1+iF^{rr})\mathbf{R}_{m+1} + i\tilde{F}^{rt}T_{m+1}] . \end{aligned} \tag{A1}$$

Here the notation is that of Ref. 27: $\mathbf{T}_m$ is the wave [$(\mathbf{k},\omega)$ Fourier component] incident *from above* on the mth layer in the incident $\mathbf{k}_t = \mathbf{k}_0$ channel [see Fig. 13(a)], $\mathbf{R}_m$ is the wave incident *from below* on the mth layer in the reflected $\mathbf{k}_r$ channel, and $i\tilde{F}^{ss'}$ is the dimensionless 2×2 planar reflection amplitude for scattering $\mathbf{k}_{s'}$ radiation into $\mathbf{k}_s$ radiation. The matrix elements of $\tilde{F}^{ss'}$ are explicitly $F^{ss'}_{ab} = n\lambda d f(\mathbf{k}_s, \hat{\boldsymbol{\epsilon}}^s_a; \mathbf{k}_{s'}, \hat{\boldsymbol{\epsilon}}^{s'}_b)/\phi_0$, where f is the atomic scattering amplitude [given by Eq. (4) for forward scattering].

As indicated schematically in Fig. 13(b), the first relation in (A1) simply states that the total wave ($\mathbf{T}_m$) incident on the mth layer from above in the t channel is equal to the total amplitude ($\mathbf{T}_{m-1}$) incident on the $m-1$ layer plus the forward scattering of this wave by the $m-1$ layer ($i\tilde{F}^{tt}T^{(t)}_{m-1}$) plus the amplitude ($iF^{tr}R_{m-1}$) of the wave scattering from the r channel to the t channel by

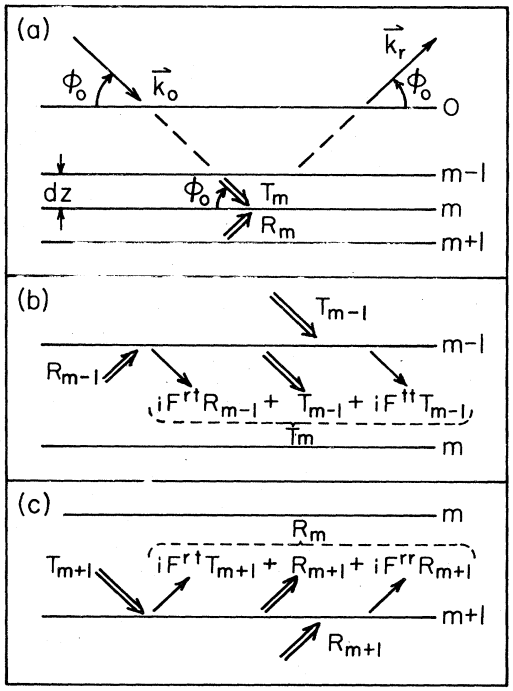

FIG. 13. (a) Schematic representation of "planar" breakup of film 1. Here the mth "plane" represents a differential layer of thickness $dz = l_1/M \to 0$. (b) Relation between T_m and T_{m-1}, R_{m-1}. (c) Relation between R_m and R_{m+1}, T_{m+1}.

the $(m-1)$ layer. All these effects are propagated to the mth layer by the phase factor $e^{ig_0 d}$. Similarly, the second relation in (A1) relating R_m to the r- and t-channel waves at the $m+1$ layer has the simple interpretation indicated in Fig. 13(c).

For grazing incidence, $\tilde{F}^{tr} = \tilde{F}^{rt} = \tilde{F}^{rr} = \tilde{F}^{tt} \equiv F$ to terms of order ϕ.[27] With this approximation, the optical equations can be simultaneously diagonalized. If film 1 is nonresonant, then *any* polarization basis will diagonalize the equations. More generally we will assume that either film 1 or one of the lower layers is resonant. Then for incident $\hat{\boldsymbol{\epsilon}}_\eta$ eigenpolarization of the *resonant* medium,[33] the basic equations for the wave amplitudes in film 1 are now the scalar equations

$$\begin{aligned} T^\eta_m &= e^{ig_0 d}\{[1+iF(\eta)]T^\eta_{m-1} + iF(\eta)R^\eta_{m-1}\} , \\ R^\eta_m &= e^{ig_0 d}\{[1+iF(\eta)]R^\eta_{m+1} + iF(\eta)T^\eta_{m+1}\} . \end{aligned} \tag{A2}$$

These finite-difference equations can be converted to differential equations with $d \to dz$, $T_m \to T(z)$, $R_m \to R(z)$, and $F \to G dz$ [$G = n\lambda f(\eta)/\phi_0$], giving

$$\begin{aligned} \frac{dT(z)}{dz} &= i(g_0+G)T(z) + iGR(z) , \\ -\frac{dR(z)}{dz} &= i(g_0+G)R(z) + iGT(z) , \end{aligned} \tag{A3}$$

where here we have suppressed the polarization index η. These equations have the immediate solutions,

$$T(z)=t_{(+)}e^{ig_1z}+t_{(-)}e^{-ig_1z}\,,$$
$$R(z)=r_{(+)}e^{ig_1z}+r_{(-)}e^{-ig_1z}\,, \tag{A4}$$

where $g_1=[g_0(g_0+2G)]^{1/2}=k\phi_0\beta_1$ as given by Eq. (3).

For a unit incident amplitude $\hat{\epsilon}_\eta$, the boundary condition at the upper surface is simply

$$T(z=0)=1\,, \tag{A5}$$

while at the interface of film 1 and medium 2 the boundary condition is

$$R(z=l_1)=R_{02}^{\dagger}(\eta)T(z=l_1)\,. \tag{A6}$$

Here, $R_{02}^{\dagger}(\eta)$ is the *total* vacuum-medium reflection amplitude of medium 2 for incident $\hat{\epsilon}_\eta$ eigenpolarization. If medium 2 is infinite, then the dynamical theory gives the usual expression

$$R_{02}^{\dagger}(\eta)=R_{02}(\eta)=\frac{1-\beta_2(\eta)}{1+\beta_2(\eta)}\,. \tag{A7}$$

The two boundary conditions (A5) and (A6) plus the two optical equations (A3) uniquely determine the coefficients $r_{(\pm)},t_{(\pm)}$ in (A4). After some manipulation,[34] the reflection amplitude is then given by

$$R=R(z=0)=r_{(+)}+r_{(-)}=\frac{R_{01}+R_{12}e^{i2g_1l_1}}{1+R_{01}R_{12}e^{i2g_1l_1}}\,, \tag{A8}$$

in agreement with Eq. (9).

For several films the solution can be obtained by iteration: For example, for a medium 3 coated with two films, 1 and 2, the boundary condition at the 1-2 interface is again given by (A6) but now with $R_{02}^{\dagger}$ given by (A8) (with the indices changes $1\rightarrow2$, $2\rightarrow3$). The resulting solution for two films is, of course, just that given by Eq. (12).

Although these results agree with the index-of-refraction results, the dynamical theory still has a somewhat different appearance. In particular, for a single infinite media ($l_1\rightarrow\infty$), the dynamical theory is still a *two-wave* theory with internal t- and r-channel waves,

$$T(z)=t_{(+)}e^{ig_1z}\,,$$
$$R(z)=r_{(+)}e^{ig_1z}\,, \tag{A9}$$

with $t_{(+)}=1$, $r_{(+)}=(1-\beta_1)/(1+\beta_1)$ ($r_{(-)}=t_{(-)}=0$ in the limit $l_1\rightarrow\infty$), whereas in the index-of-refraction approach there is a *single* internal wave,

$$\mathbf{A}_T(z)=\hat{\epsilon}_1t_{01}e^{ig_1z}\,, \tag{A10}$$

with $t_{01}=2/(1+\beta_1)$ (see Fig. 14). There is of course no discrepancy here: In the dynamical theory the *total* wave field at z is in fact a wave traveling in the refracted direction $\mathbf{k}_1$, with polarization $\hat{\epsilon}_1$ and with the refraction angle ϕ_1 determined by Snell's law $N_1\cos\phi_1=\cos\phi_0$, i.e., by direct substitution from (A9),

$$\mathbf{A}_T(z)\equiv\hat{\epsilon}_0T(z)+\hat{\epsilon}_rR(z)$$
$$=\hat{\epsilon}_1t_{01}e^{ig_1z}[1+O(1-N_1)]\,. \tag{A11}$$

Here the correction terms are of order $(1-N_1)\approx10^{-5}$, which is the same order of magnitude of the other approximations in the theory.

APPENDIX B

There is extensive literature on thin-film interference techniques for optical reflections from thin dielectric films[1-6] and these ideas can be taken over directly to x-ray grazing incidence (within the limits imposed by strong photoabsorption). However, almost all the theory for thin-film optical filters is expressed in terms of the "characteristic matrices" $\tilde{\mathcal{M}}_n$ which relate the tangential E and B fields at the adjacent boundaries of the nth film.

In order to make this literature more accessible to our case, we summarize the main results, making the appropriate modifications for x-ray grazing incidence. For nonmagnetic dielectric films, the tangential components of **E** and **B** are continuous across each boundary. For the mth film, E_m and B_m designate the *tangential* components of the *total* **E** and **B** fields at the upper interface (see Fig. 15) and E_{m+1},B_{m+1} are the fields at the lower interface. It is straightforward to show that the fields at adjacent boundaries are related by[1,4]

$$\begin{bmatrix}E_m\\B_m\end{bmatrix}=\tilde{\mathcal{M}}_m\begin{bmatrix}E_{m+1}\\B_{m+1}\end{bmatrix}\,, \tag{B1}$$

where $\tilde{\mathcal{M}}_m$ is the characteristic matrix for the mth film,

$$\tilde{\mathcal{M}}_m=\begin{bmatrix}\cos\delta_m & i\sin\delta_m/\eta_m\\ i\eta_m\sin\delta_m & \cos\delta_m\end{bmatrix}\,, \tag{B2}$$

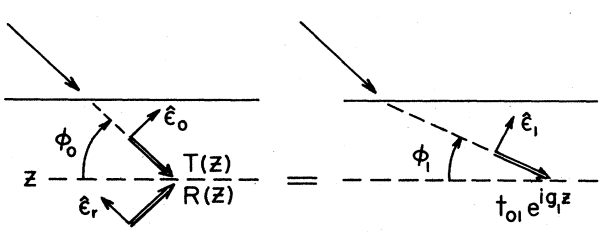

FIG. 14. Equivalence of two-wave dynamical treatment and the single-wave refraction treatment.

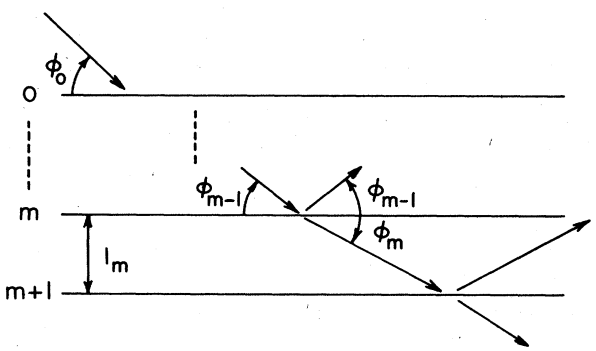

FIG. 15. Multilayer film geometry.

and where here

$$\delta_m = k_0 l_m N_m \sin\phi_m \simeq g_m l_m \ , \tag{B3}$$

with $g_m = k_0 \phi_0 \beta_m$ as given in Eqs. (2) and (3), and

$$\eta_m^{(\sigma)} = N_m \sin\phi_m \simeq \phi_0 \beta_m \ ,$$
$$\eta_m^{(\pi)} = N_m / \sin\phi_m \simeq (\phi_0 \beta_m)^{-1} \ , \tag{B4}$$

for σ and π polarization, respectively. In (B3) and (B4), $N_m = 1 + 2\pi \hat{\lambda}^2 n f \simeq (1 - 10^{-5})$ is the index of refraction of the mth film, and to get the final form, we have used Snell's law for parallel interfaces, $N_m \cos\phi_m = N_0 \cos\phi_0$.

For a series of p films plus substrate s, the characteristic matrix $\tilde{\mathcal{M}}$ for the entire series (which relates the total E_0 and B_0 at the top surface to $E_{p+1} = E_s$, $B_{p+1} = B_s$ at the substrate surface) is then

$$\tilde{\mathcal{M}} = \tilde{\mathcal{M}}_1 \cdots \tilde{\mathcal{M}}_p = \begin{bmatrix} m_{11} & m_{12} \\ m_{21} & m_{22} \end{bmatrix} \tag{B5}$$

and the amplitude of the reflected wave is given by[4]

$$R = \frac{\eta_0 m_{11} + \eta_0 \eta_s m_{12} - m_{21} - \eta_s m_{22}}{\eta_0 m_{11} + \eta_0 \eta_s m_{12} + m_{21} + \eta_s m_{22}} \ , \tag{B6}$$

where η_0 ($= \phi_0$ or ϕ_0^{-1}) and η_s are defined by (B4). Thus, to get R for any configuration of films, the procedure is simply to calculate $\tilde{\mathcal{M}}_m$ for each film, multiply in sequential order to get $\tilde{\mathcal{M}}$, and substitute into (B6).

This is a straightforward procedure and gives a closed expression for any series of films. Furthermore, in the absence of absorption, the character matrix $\tilde{\mathcal{M}}_m$ is very simple for a half-wave film [$\delta_m = (2n+1)\pi$ and $\tilde{\mathcal{M}}_m$ is diagonal and equal to -1] or for a quarter-wave film [$\delta_m = (2n+1)\pi/2$ and the diagonal elements of $\tilde{\mathcal{M}}_m$ are zero], which makes the analysis for a series of half- and quarter-wave films particularly easy. The disadvantage of this approach is that the physics is obscured and, moreover, in the presence of strong absorption, the special simplicity of $\tilde{\mathcal{M}}$ for half- and quarter-wave films is lost.

As a particular example of the formalism for a single film 1 on a substrate 2, $\tilde{\mathcal{M}} = \tilde{\mathcal{M}}_1$ is given by (B2), $\eta_0 = \phi_0$, $\eta_s = \phi_0 \beta_2$ (taking σ polarization), giving

$$R = \frac{\cos(g_1 l_1)(1-\beta_2) + i \sin(g_1 l_1)(\beta_2/\beta_1 - \beta_1)}{\cos(g_1 l_1)(1+\beta_2) + i \sin(g_1 l_1)(\beta_2/\beta_1 + \beta_1)} \ . \tag{B7}$$

With some manipulation, Eq. (B7) can be shown to be equivalent to Eq. (9). The condition for an antireflection film $R = 0$ gives the condition

$$\tan(g_1 l_1) = -i(1-\beta_2)/(\beta_2/\beta_1 - \beta_1) \ , \tag{B8}$$

which has no obvious interpretation. However, by making use of $\tanh^{-1} z = \ln\sqrt{(1+z)/(1-z)}$, the condition can be transformed to

$$i g_1 l_1 = \tfrac{1}{2} \ln(-R_{01}/R_{12}) \ , \tag{B9}$$

where R_{01}, R_{12} are the interface reflection amplitudes. The real and imaginary parts of (B9) give the impedance-match and destructive interference conditions of Eqs. (20) and (22). Either approach leads to the same results, but the interface reflection approach is more intuitive.

[1] H. A. Macleod, *Thin Film Optical Filters* (American Elsevier, New York, 1969) and references therein.

[2] J. T. Cox and G. Hass, in *Physics of Thin Films,* edited by G. Hass and R. E. Thun (Academic, New York, 1964), Vol. 2, pp. 239–304.

[3] A. Vasicek, *Optics of Thin Films* (North-Holland, Amsterdam, 1960).

[4] E. Hecht and A. Zajac, *Optics* (Addison-Wesley, Reading, Mass., 1974), pp. 311–316.

[5] M. Born and E. Wolf, *Principles of Optics* (Pergamon, New York, 1959), pp. 50–69.

[6] P. Bowmeister and G. Pincus, Sci. Am. **223**, 59 (1970).

[7] E. Spiller, Appl. Phys. Lett. **20**, 365 (1972).

[8] R.-P. Haelbich and C. Kunz, Opt. Commun. **17**, 287 (1976).

[9] A. V. Vinogradov and B. Ya. Zeldovich, Appl. Opt. **16**, 89 (1977).

[10] R.-P. Haelbich, A. Segmüller, and E. Spiller, Appl. Phys. Lett. **34**, 184 (1979).

[11] E. Spiller, A. Segmüller, J. Rife, and R.-P. Haelbich, Appl. Phys. Lett. **37**, 1048 (1980).

[12] F. Mezei, Commun. Phys. **1**, 81 (1976); **2**, 41(E) (1977).

[13] A. M. Saxena and B. P. Schoenborn, Acta Crystallogr. Sect. A **33**, 805 (1977).

[14] J. P. Hannon, G. T. Trammell, M. Mueller, E. Gerdau, H. Winkler, and R. Rüffer, Phys. Rev. Lett. **43**, 636 (1979).

[15] A. H. Compton, Philos. Mag. **45**, 1121 (1923).

[16] H. Kiessig, Ann. Phys. (Leipzig) **10**, 715 (1931); **10**, 769 (1931).

[17] A. I. Alichanow and L. A. Arzimowic, Z. Phys. **82**, 489 (1933).

[18] L. G. Parratt, Phys. Rev. **95**, 359 (1954).

[19] L. M. Rieser, J. Opt. Soc. Am. **47**, 987 (1957).

[20] A. Segmüller, Thin Solid Films **18**, 287 (1973).

[21] J. P. Hannon, N. V. Hung, G. T. Trammell, E. Gerdau, M. Mueller, R. Rüffer, and H. Winkler, following paper (II), Phys. Rev. B **32**, 5081 (1985).

[22] J. P. Hannon *et al.*, paper III, Phys. Rev. B (to be published).

[23] J. P. Hannon *et al.*, paper IV, Phys. Rev. B (to be published).

[24] J. P. Hannon, J. T. Hutton, G. T. Trammell, E. Gerdau, and R. Rüffer, paper V (unpublished).

[25] J. P. Hannon, J. T. Hutton, G. T. Trammell, E. Gerdau, and R. Rüffer, paper VI (unpublished).

[26] G. T. Trammell, *Chemical Effects of Nuclear Transformations* (International Atomic Energy Agency, Vienna, 1961), Vol. 1, p. 75.

[27] J. P. Hannon and G. T. Trammell, Phys. Rev. **186**, 306 (1969).

[28] J. P. Hannon, N. J. Carron, and G. T. Trammell, Phys. Rev. B **9**, 2810 (1974), p. 2828.

[29] E.g., R. W. James, *The Optical Principles of the Diffraction of X-rays* (Cornell University Press, Ithaca, 1965), pp. 167, 171-190, and 426-435.

[30] G. Materlik (private communication).

[31] M. Harsdorff (private communication).

[32] See Appendix D of Ref. 27.

[33] For the explicit expression for the eigenpolarizations, see Refs. 22 or 27.

[34] Here it is useful to note the addition rule that $(R_{10} + R_{02})/(1 + R_{10} R_{02}) = R_{12}$.